Inorg. Chem. **2005**, *44*, 2098–2105

Reactions of a Gallium(II)–Diazabutadiene Dimer, $[\{\{[(H)C(Bu^t)N]_2\}GaI\}_2]$, with $[ME(SiMe_3)_2]$ (M = Li or Na; E = N, P, or As): Structural, EPR, and ENDOR Characterization of Paramagnetic Gallium(III) Pnictide Complexes

Karen L. Antcliff, Robert J. Baker, Cameron Jones,* Damien M. Murphy,* and Richard P. Rose

Center for Fundamental and Applied Main Group Chemistry, School of Chemistry, Cardiff University, P.O. Box 912, Park Place, Cardiff CF10 3TB, United Kingdom

Received September 20, 2004

The reactions of the paramagnetic gallium(II) complex $[\{(Bu^t\text{-DAB})GaI\}_2]$ (Bu^t-DAB = $\{(Bu^t)NC(H)\}_2$) with the alkali metal pnictides $[ME(SiMe_3)_2]$ (M = Li or Na; E = N, P, or As) have been carried out under a range of stoichiometries. The 1:2 reactions have led to a series of paramagnetic gallium(III)–pnictide complexes, $[(Bu^t\text{-DAB})Ga\{E(SiMe_3)_2\}I]$ (E = N, P, or As), while two of the 1:4 reactions afforded $[(Bu^t\text{-DAB})Ga\{E(SiMe_3)_2\}_2]$ (E = P or As). In contrast, treatment of $[\{(Bu^t\text{-DAB})GaI\}_2]$ with 4 equiv of $[NaN(SiMe_3)_2]$ resulted in a novel gallium heterocycle coupling reaction and the formation of the diradical species $[(Bu^t\text{-DAB})Ga\{N(SiMe_3)_2\}\{[CC(H)N_2(Bu^t)_2]\text{-}Ga[N(SiMe_3)_2]CH_3\}]$. The mechanism of this unusual reaction has been explored, and evidence suggests it involves an intramolecular transmethylation reaction. The X-ray crystal structures of all prepared complexes are reported, and all have been characterized by EPR and ENDOR spectroscopies. The observed spin Hamiltonian parameters provide a detailed picture of the distribution of the unpaired spin density over the molecular frameworks of the complexes.

Introduction

The chemistry of gallium(III) pnictide complexes is very well developed.[1] In this field the bis(silyl)pnictide ligands, $[E(SiMe_3)_2]^-$, E = N, P, As, or Sb, are especially important, as their gallium complexes have been widely used as precursors to the binary gallium pnictides, GaE, via thermal decomposition pathways.[1,2] Recently, this chemistry has been extended to gallium(I) with the reactions of $[LiN(SiMe_3)_2]$ with "metastable" gallium(I) halides, $[\{GaX(L)\}_n]$, X = halide and L = ether, amine, or phosphine. These lead to an array of remarkable suboxidation state "metalloid" cluster compounds, e.g. $[Ga_{84}\{N(SiMe_3)_2\}_{20}]$,$^{4-}$ via controlled disproportionation reactions.[3] Related clusters derived from the dialkyl phosphide ligand, $[PBu^t_2]^-$, have also been described in the last 2 years, e.g. $[Ga_{16}(PBu^t_2)_{10}]$[4] and $[Ga_{51}(PBu^t_2)_{14}\text{-}Br_6]^{3-}$.[5] In gallium(II) chemistry, amide complexes are rare[6] and, to the best of our knowledge, there is only one structurally characterized phosphide complex[7] and no known arsenides. Of the known crystallographically authenticated gallium(II) complexes, the $[E(SiMe_3)_2]^-$ ligands have not been featured. Considering their importance to Ga(III)

* Authors to whom correspondence should be addressed. E-mail: Jonesca6@cardiff.ac.uk (C.J.); murphydm@cardiff.ac.uk (D.M.M.).

(1) E.g.: (a) Carmalt, C. J. *Coord. Chem. Rev.* **2001**, *223*, 217. (b) Schulz, S. *Coord. Chem. Rev.* **2001**, *215*, 1. (c) Wells, R. L. *Coord. Chem. Rev.* **1992**, *112*, 273. (d) Taylor, M. J.; Brothers, P. J. In *Chemistry of Aluminium, Gallium, Indium and Thallium*; Downs, A. J., Ed.; Chapman and Hall: London, 1993; pp 517−524. (e) Lappert, M. F.; Power, P. P.; Senger, A. R.; Srivastava, R. C. *Metal and Metalloid Amides*; Ellis-Horwood: Chichester, U.K., 1980; and references therein.

(2) E.g.: (a) Carmalt, C. J.; Mileham, J. D.; White, A. J. P.; Williams, D. J. *Dalton Trans.* **2003**, 4255. (b) Jouet, R. J.; Wells, R. L.; Rheingold, A. L.; Incarvito, C. D. *J. Organomet. Chem.* **2000**, *601*, 191. (c) Janik, J. F.; Baldwin, R. A.; Wells, R. L.; Pennington, W. T.; Schimek, G. L.; Rheingold, A. L.; Liable-Sands, L. M. *Organometallics* **1996**, *15*, 5385. (d) Barry, S. T.; Richeson, D. S. *Chem. Mater.* **1994**, *6*, 2220.

(3) Schnepf, A.; Schnöckel, H.-G. *Angew. Chem., Int. Ed.* **2002**, *41*, 3532 and references therein.

(4) Steiner, J.; Stösser, G.; Schnöckel, H.-G. *Angew. Chem., Int. Ed.* **2003**, *42*, 1971.

(5) Steiner, J.; Stösser, G.; Schnöckel, H.-G. *Angew. Chem., Int. Ed.* **2004**, *43*, 302.

(6) (a) Linti, G.; Kotsler, W.; Rodig, A. *Z. Anorg. Allg. Chem.* **2002**, *628*, 1319. (b) Schmidt, E. S.; Schier, A.; Mitzel, N. W.; Schmidbaur, H. *Z. Naturforsch. B* **2001**, *56*, 458. (c) Pott, T.; Jutzi, P.; Schoeller, W. W.; Stammler, A.; Stammler, H. G. *Organometallics* **2001**, *20*, 5492. (d) Linti, G.; Frey, R.; Schmidt, M. *Z. Naturforsch. B* **1994**, *49*, 958.

(7) Li, W. W.; Wei, P.; Beck, B. C.; Xie, Y.; Schaefer, H. F., III; Su, J.; Robinson, G. H. *Chem. Commun.* **2000**, 453.

10.1021/ic0486825 CCC: $30.25
Published on Web 02/11/2005

Chart 1[a]

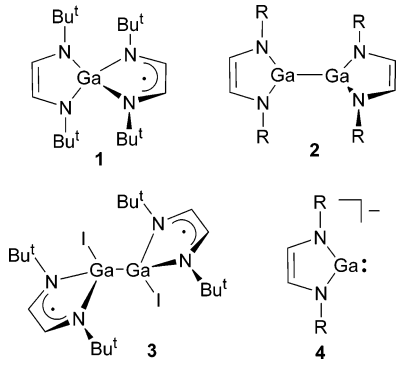

[a] R = Bu^t or $C_6H_3Pr^i_2$-2,6.

chemistry and the amide's ability to stabilize suboxidation state gallium clusters, it was our intention to prepare gallium(II)−bis(silyl)pnictide complexes and investigate their properties.

The ability of the diazabutadiene class of ligand to stabilize diamagnetic and paramagnetic gallium complexes with the metal in a variety of oxidation states, e.g. **1**−**4** (Chart 1), is now well-known.[6c,8−11] In our group, and that of Schmidbaurs, this ability has been most evidently exploited in the formation of the valence isoelectronic N-heterocyclic carbene analogues, **4**, the coordination chemistry of which is currently emerging.[12] As a component of those studies, we have developed a synthetic route to **3**, which we have used as a precursor to **4**, R = Bu^t.[10] Additionally, we saw **3** as a potential precursor to gallium(II) pnictide complexes. To this end, the reactivity of [{(Bu^t-DAB)GaI}$_2$], **3** (Bu^t-DAB = {(Bu^t)NC(H)}$_2$), toward [ME(SiMe$_3$)$_2$] (M = Li or Na; E = N, P, or As) has been examined. The unexpected results of this study are reported here.

Experimental Section

General Methods. All manipulations were carried out using standard Schlenk and glovebox techniques under an atmosphere of high-purity argon. Diethyl ether and hexane were distilled over Na/K alloy, toluene-d_8 was distilled over potassium, and CD_2Cl_2 was distilled over CaH_2 and then freeze/thaw degassed prior to use. The continuous wave (CW) EPR/ENDOR spectra were recorded on an X-band Bruker ESP300E series spectrometer equipped with an ESP360 DICE ENDOR unit, operating at 12.5 kHz field modulation in a Bruker EN801 cavity. The ENDOR spectra were recorded at 10 K using an Oxford instruments ESR 900 continuous-flow He Cryostat. The ENDOR spectra were obtained using 8 dB rf power from a ENI A-300 RF amplifier with 75 or 250 kHz rf modulation depth. Computer simulations were carried out using Bruker's Simfonia program.[13] Mass spectra were recorded using a VG Fisons Platform II instrument under APCI conditions. IR spectra were recorded using a Nicolet 510 FT-IR spectrometer as Nujol mulls between NaCl plates. Melting points were determined in sealed glass capillaries under argon and are uncorrected. Microanalyses were obtained from Medac Ltd. [{(Bu^t-DAB)GaI}$_2$],[10] [NaN(SiMe$_3$)$_2$],[14] [LiP(SiMe$_3$)$_2$.DME],[15] and [LiAs(SiMe$_3$)$_2$.DME][15] were synthesized by literature procedures.

Preparation of [(Bu^t-DAB)Ga{N(SiMe$_3$)$_2$}I] (5). To a solution of [{(Bu^t-DAB)GaI}$_2$] (0.30 g, 0.41 mmol) in Et$_2$O (15 cm^3) was added [NaN(SiMe$_3$)$_2$] (0.15 g, 0.83 mmol) in Et$_2$O (15 cm^3) at −78 °C over 5 min. The resultant solution was warmed to room temperature and stirred overnight to yield a yellow solution and white precipitate. Volatiles were removed in vacuo, and the residue was extracted with hexane (20 cm^3). Filtration, concentration, and cooling to −30 °C overnight yielded orange crystals of **5** (0.10 g, 46%). Mp: 154−156 °C. IR (ν/cm^{-1}; Nujol): 1262 (s), 1202 (s), 919 (sh), 883 (sh), 829 (s), 775 (w), 760 (w), 721 (s), 669 (w). MS (*m*/*z*; APCI): 524 [M$^+$, 100%], 397 [M$^+$ − I, 55%], 169 [Bu^t − DABH$^+$, 23%]. Anal. Calcd for $C_{16}H_{38}N_3GaSi_2I$: C, 36.58; H, 7.29; N, 8.00. Found: C, 36.11; H, 7.36; N, 8.31.

Preparation of [(Bu^t-DAB)Ga{P(SiMe$_3$)$_2$}I] (6). To a solution of [{(Bu^t-DAB)GaI}$_2$] (0.30 g, 0.41 mmol) in Et$_2$O (15 cm^3) was added [LiP(SiMe$_3$)$_2$.DME] (0.22 g, 0.82 mmol) in Et$_2$O (15 cm^3) at −78 °C over 5 min. The resultant solution was warmed to room temperature and stirred overnight to yield a red solution. Volatiles were removed in vacuo, and the residue was extracted with hexane (20 cm^3). Filtration, concentration, and cooling to −30 °C overnight yielded red crystals of **6** (0.10 g, 45%). Mp: 124−126 °C. IR (ν/cm^{-1}; Nujol): 1261 (m), 1206 (w), 1096 (w), 1018 (w), 719 (m). MS (*m*/*z*; APCI): 414 [M$^+$ − I, 20%], 365 [M$^+$ − P(SiMe$_3$)$_2$, 31%], 169 [Bu^t-DABH$^+$, 100%].

Preparation of [(Bu^t-DAB)Ga{As(SiMe$_3$)$_2$}I] (7). To a solution of [{(Bu^t-DAB)GaI}$_2$] (0.30 g, 0.41 mmol) in Et$_2$O (15 cm^3) was added [LiAs(SiMe$_3$)$_2$.DME] (0.26 g, 0.82 mmol) in Et$_2$O (15 cm^3) at −78 °C over 5 min. The resultant solution was warmed to room temperature and stirred overnight to yield a red solution. Volatiles were removed in vacuo, and the residue was extracted with hexane (20 cm^3). Filtration, concentration, and cooling to −30 °C overnight yielded red crystals of **7** (0.08 g, 33%). Mp: 130−132 °C. IR (ν/cm^{-1}; Nujol): 1457 (s), 1368 (s), 1361 (s), 1328 (sh), 1262 (s), 1244 (s), 1213 (s), 836 (m), 776 (s), 747 (s), 691 (s), 620 (s). MS (*m*/*z*; APCI): 291 [GaAs(SiMe$_3$)$_2^+$, 10%], 221 [As(SiMe$_3$)$_2^+$, 5%], 169 [Bu^t-DABH$^+$, 100%]. Anal. Calcd for $C_{16}H_{38}N_2GaAsSi_2I$: C, 32.78; H, 6.53; N, 4.78. Found: C, 32.16; H, 6.59; N, 4.51.

Preparation of [(Bu^t-DAB)Ga{P(SiMe$_3$)$_2$}$_2$] (8). To a solution of [{(Bu^t-DAB)GaI}$_2$] (0.30 g, 0.41 mmol) in Et$_2$O (15 cm^3) was added LiP(SiMe$_3$)$_2$·DME (0.45 g, 1.60 mmol) in Et$_2$O (15 cm^3) at −78 °C over 5 min. The resultant solution was warmed to room temperature and stirred overnight. Volatiles were removed in vacuo, and the residue was extracted with hexane (20 cm^3). Filtration, concentration, and cooling to −30 °C overnight yielded red crystals of **8** (0.08 g, 33%). Mp: 160−162 °C. IR (ν/cm^{-1}; Nujol): 1369 (s), 1337 (s), 1262 (sh), 1243 (s), 1210 (s), 937 (s), 832 (m), 744 (s), 680 (s). MS (*m*/*z*; APCI): 593 [M$^+$, 65%], 415 [M$^+$ − P(SiMe$_3$)$_2$, 75%], 169 [Bu^t-DABH$^+$, 100%]. Anal. Calcd for

(8) (a) Cloke, F. G. N.; Hanson, G. R.; Henderson, M. J.; Hitchcock, P. B.; Raston, C. L. *J. Chem. Soc, Dalton Trans.* **1989**, 1002. (b) Kaim, W.; Matheis, W. *J. Chem. Soc., Chem. Commun.* **1991**, 597. (c) Power, P. *Chem. Rev.* **2003**, *103*, 789 and references therein.

(9) Brown, D. S.; Decken, A.; Cowley, A. H. *J. Am. Chem. Soc.* **1995**, *117*, 7, 5421.

(10) (a) Baker, R. J.; Farley, R. D.; Jones, C.; Kloth, M.; Murphy, D. M. *J. Chem. Soc., Dalton Trans.* **2002**, 3844, (b) Baker, R. J.; Farley, R. D.; Jones, C.; Mills, D. P.; Kloth, M.; Murphy, D. M. *Chem.*−*Eur. J.*, in press.

(11) (a) Schmidt, E. S.; Jockisch, A.; Schmidbaur, H. *J. Am. Chem. Soc.* **1999**, *121*, 9578. (b) Schmidt, E. S.; Schier, A.; Schmidbaur, H. *J. Chem. Soc., Dalton Trans.* **2001**, 505.

(12) (a) Baker, R. J.; Jones, C.; Kloth, M.; Platts, J. A. *Angew. Chem., Int. Ed.* **2003**, *42*, 2660. (b) Baker, R. J.; Jones, C.; Platts, J. A. *J. Am. Chem. Soc.* **2003**, *125*, 10534. (c) Baker, R. J.; Jones, C.; Platts, J. A. *J. Chem. Soc., Dalton Trans.* **2003**, 3673. (d) Baker, R. J.; Jones, C.; Kloth, M.; Platts, J. A. *Organometallics* **2004**, *23*, 4811.

(13) *WINEPR SIMFONIA*, version 1.25; Brüker Analytische: Messtechnick, Germany, 1996.

(14) Clark, D. L.; Sattelberger, A. P. *Inorg. Synth.* **1997**, *31*, 307.

(15) Fritz, G.; Hoelderich, W. *Z. Anorg. Allg. Chem.* **1976**, *422*, 104.

Table 1. Summary of Crystallographic Data for Compounds **5**−**10**

	5	**6**	**7**	**8**	**9**	**10**
empirical formula	$C_{16}H_{38}GaIN_3Si_2$	$C_{16}H_{38}GaIN_2PSi_2$	$C_{16}H_{38}AsGaIN_2Si_2$	$C_{22}H_{56}GaN_2P_2Si_4$	$C_{22}H_{56}As_2GaN_2Si_4$	$C_{33}H_{78}Ga_2N_6Si_4$
fw	525.29	542.25	586.20	592.71	680.61	810.81
cryst system	orthorhombic	monoclinic	monoclinic	monoclinic	monoclinic	orthorhombic
space group	Pnma	$P2_1/c$	$P2_1/c$	$P2/c$	$C2/c$	$Pna2_1$
a (Å)	18.408(4)	15.011(3)	15.009(3)	31.505(6)	65.250(13)	25.772(5)
b (Å)	14.517(3)	18.299(4)	18.462(4)	9.822(2)	9.859(2)	15.892(3)
c (Å)	8.9790(18)	9.2890(19)	9.3350(19)	16.731(3)	16.775(3)	11.214(2)
β (deg)	90	92.58(3)	92.77(3)	90.69(3)	103.72(3)	90
V (Å^3)	2399.4(8)	2549.0(9)	2583.7(9)	5176.9(18)	10483(4)	4592.9(16)
Z	4	4	4	6	12	4
ρ(calcd) (g·cm^{-3})	1.454	1.413	1.507	1.141	1.294	1.173
μ (mm^{-1})	2.537	2.449	3.625	1.042	2.817	1.305
F(000)	1068	1100	1172	1914	4260	1744
cryst size (mm)	0.25 × 0.25 × 0.20	0.30 × 0.15 × 0.10	0.35 × 0.25 × 0.15	0.30 × 0.25 × 0.20	0.30 × 0.25 × 0.20	0.25 × 0.25 × 0.15
θ range (deg)	3.17−27.47	2.94−27.48	2.93−27.14	3.08−26.02	3.05−26.36	3.01−25.32
reflcns collcd	13 527	18 139	16 234	31 339	35 496	19 377
R_{int}	0.0533	0.0724	0.1266	0.0802	0.0795	0.0652
data/restraints/params	2847/0/123	5798/0/221	5522/0/221	10 138/24/479	10 518/18/479	7754/1/433
goodness of fit on F^2	1.034	1.022	1.020	1.050	1.026	1.024
R1[a] indices [$I > 2\sigma(I)$]	0.0283	0.0424	0.0766	0.0551	0.0456	0.0543
wR2[a] indices (all data)	0.0608	0.0868	0.2097	0.1391	0.1012	0.1274
largest peak and hole (e·Å^{-3})	0.487/−0.660	0.838/−0.534	2.814 (near As1)/ −2.045 (near I1)	1.135/−0.580	0.874/−0.628	1.830 (near Ga1)/ −0.435

[a] $R1(F) = \{\Sigma(|F_o| - |F_c|)/\Sigma|F_o|\}$ for reflections with $F_o > 4(\sigma(F_o))$. $wR2(F^2) = \{\Sigma w(|F_o|^2 - |F_c|^2)^2/\Sigma w|F_o^2|^2\}^{1/2}$, where w is the weight given each reflection.

Table 2. Selected Metrical Parameters for Complexes **5**−**9**

	av Ga−N (Bu^t-DAB) (Å)	Ga−I (Å)	Ga−E (Å)	N−Ga−N (deg)	Σ angles at E (deg)	av C−N (in heterocycle) (Å)	C−C (in heterocycle) (Å)
5	1.956	2.5906(5)	1.868(2)	85.86(11)	360.0	1.329	1.406(5)
6	1.963	2.5893(8)	2.2991(11)	85.88(13)	323.3	1.326	1.395(6)
7	1.957	2.5944(12)	2.3893(12)	85.6(3)	316.8	1.318	1.411(12)
8	1.986		2.343 (av)	84.74(15)	330.4 (av)	1.330	1.394(6)
9	1.991		2.437 (av)	84.62(14)	322.6 (av)	1.328	1.382(6)

$C_{22}H_{56}N_2GaP_2Si_4$: C, 43.58; H, 9.52; N, 4.73. Found: C, 43.90; H, 9.73; N, 4.84.

Preparation of [(Bu^t-DAB)Ga{As(SiMe$_3$)$_2$}$_2$] (9). To a solution of [{(Bu^t-DAB)GaI}$_2$] (0.30 g, 0.41 mmol) in Et_2O (15 cm^3) was added a solution of $LiAs(SiMe_3)_2$·DME (0.52 g, 1.60 mmol) in Et_2O (15 cm^3) at −78 °C over 5 min. The resultant solution was warmed to room temperature and stirred overnight to yield a red solution. Volatiles were removed in vacuo, and the residue was extracted with hexane (20 cm^3). Filtration, concentration, and cooling to −30 °C overnight yielded red crystals of **9** (0.15 g, 54%). Mp: 158−160 °C. IR (ν/cm^{-1}; Nujol): 1458 (s), 1376 (s), 1260 (w), 1241 (w), 1208 (w), 834 (m), 722 (w). MS (*m*/*z*; APCI): 680 [M$^+$, 18%], 624 [M$^+$ − Bu^t, 18%], 459 [M$^+$ − As(SiMe$_3$)$_2$, 32%], 169 [Bu^t-DABH$^+$, 100%]. Anal. Calcd for $C_{22}H_{56}N_2GaAs_2Si_4$: C, 38.82; H, 8.29; N, 4.12. Found: C, 38.33; H, 8.37; N, 4.13.

Preparation of [(Bu^t-DAB)Ga{N(SiMe$_3$)$_2$}{[CC(H)N$_2$(Bu^t)$_2$]-Ga[N(SiMe$_3$)$_2$]CH$_3$}] (10). To a solution of [{(Bu^t-DAB)GaI}$_2$] (0.30 g, 0.41 mmol) in Et_2O (15 cm^3) was added [NaN(SiMe$_3$)$_2$] (0.30 g, 1.60 mmol) in Et_2O (15 cm^3) at −78 °C over 5 min. The resultant solution was warmed to room temperature and stirred overnight to yield a brown suspension. Volatiles were removed in vacuo, and the residue was extracted with hexane (20 cm^3). Filtration, concentration, and cooling to −30 °C overnight yielded olive crystals of **10** (0.10 g, 30%). Mp: 123−125 °C. IR (ν/cm^{-1}; Nujol): 1295 (w), 1244 (w), 1200 (w), 957 (s), 904 (w), 875 (s), 833 (w), 721 (w), 669 (m). MS (*m*/*z*; APCI): 413 [(Bu^t-DAB)Ga-(Me){N(SiMe$_3$)$_2$}$^+$, 14%], 398 [(Bu^t-DAB)Ga{N(SiMe$_3$)$_2$}$^+$, 4%], 252 [(Bu^t-DAB)GaMe$^+$, 16%], 161 [N(SiMe$_3$)$_2$H$^+$, 100%].

X-ray Crystallography. Crystals of **5**−**10** suitable for X-ray structural determination were mounted in silicone oil. Crystallographic measurements were made using a Nonius Kappa CCD diffractometer using a graphite monochromator with Mo Kα radiation (λ = 0.710 73 Å). The data were collected at 150 K, and the structures were solved by direct methods and refined on F^2 by full-matrix least squares (SHELX97)[16] using all unique data. All non-hydrogen atoms are anisotropic with H atoms included in calculated positions (riding model). Crystal data and details of data collections and refinement are given in Table 1. Selected metrical parameters for **5**−**9** are compiled in Table 2.

Results and Discussion

Synthetic and Structural Studies. The reactions of **3** with 2 equiv of [ME(SiMe$_3$)$_2$] (M = Li or Na; E = N, P, or As) afforded good yields of the mono(pnictido)gallium(III) complexes, **5**−**7** (Scheme 1). The mechanism of formation of these compounds is uncertain, but it must involve salt elimination, Ga−Ga bond cleavage, and disproportionation reactions. In this respect, it is noteworthy that related reactions of organodigallium(II) diiodides, [{GaI(R)}$_2$], R = C(SiMe$_3$)$_3$, with carboxylate salts do not lead to Ga−Ga bond cleavage but to salt elimination and the formation carboxylate-bridged gallium(II) complexes, e.g. [{Ga(R)}$_2$-{μ-O$_2$C(Ph)}$_2$].[17] In the formation of **5**−**7**, the only identified byproducts were gallium metal and small amounts of the known Ga(III) complex [Ga(Bu^t-DAB)$_2$], **1**.[8] It is interesting

(16) Sheldrick, G. M. *SHELX-97*; University of Göttingen: Göttingen, Germany, 1997.
(17) (a) Uhl, W.; El-Hamdan, A. *Eur. J. Inorg. Chem.* **2004**, 969. (b) Uhl, W. *Chem. Soc. Rev.* **2000**, *29*, 259. (c) Uhl, W. *Adv. Organomet. Chem.* **2004**, *51*, 53.

Scheme 1

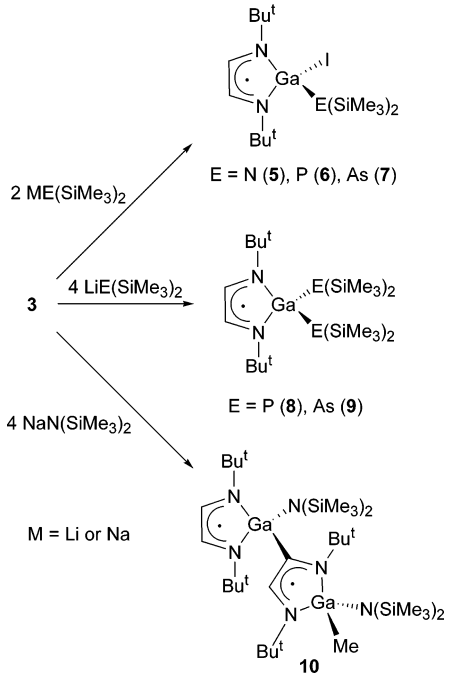

that when the reactions were carried out in 1:1 stoichiometries, **5**−**7** were formed in reduced yields and significant amounts of **3** were recovered unreacted. Therefore, it appears that the mechanism of formation of these compounds requires 2 equiv of the alkali-metal pnictide. Moreover, due to the observed disproportionation processes, it is clear that each dimeric molecule of **3** can give rise to only one molecule of monomeric **5**−**7** in these reactions. It should also be mentioned that attempts to prepare the antimonide analogue of **5**−**7** by reaction of **3** with [$LiSb(SiMe_3)_2$] were not successful and led to the formation of the known distibine $\{Sb(SiMe_3)_2\}_2$[18] via an oxidative coupling of the antimonide fragment.

Due to their paramagnetic nature, no meaningful NMR spectroscopic data could be obtained for **5**−**7**. Consequently, X-ray crystallographic studies were required to elucidate their structures. The molecular structures of **5** and **7** are depicted in Figures 1 and 2, while that for **6** was found to be isomorphous to **7** and, therefore, has been deposited as Supporting Information (see also Table 1). The geometries of the diazabutadiene ligands in **5**−**7** (Table 2) are similar to each other and are suggestive of significant delocalization, as has been found in related paramagnetic complexes, e.g. [GaI_2(Bu^t-DAB)].[10] Likewise, the geometries about the gallium centers of the complexes are comparable. The only obvious trend in the series involves the angles about the pnictide centers in **5**−**7**. As would be expected, the amido N-center in **5** is trigonal planar, while the geometries of the P- and As-centers in **6** and **7** tend toward pyramidal. The Ga−N(amide) bond length of 1.868(2) Å in **5** is greater than its Ga−N(Bu^t-DAB) interactions but identical with the Ga−N distances in [$Ga\{N(SiMe_3)_2\}_3$].[19] Complexes **6** and **7** contain rare examples of terminal phosphido− and

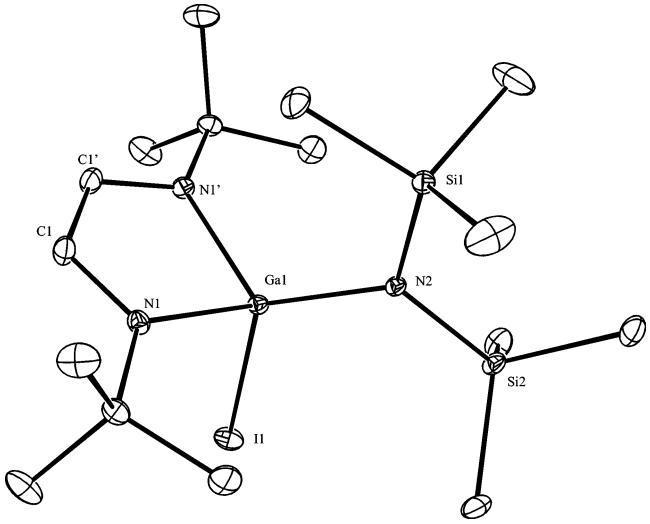

Figure 1. Thermal ellipsoid plot (30% probability surface) of the molecular structure of [(Bu^t-DAB)Ga{$N(SiMe_3)_2$}I] (**5**). Hydrogen atoms are omitted for clarity. Selected metrical parameters are listed in Table 2. Symmetry transformation used to generate equivalent atoms: ′, x, $-y + 1/2$, $-z$.

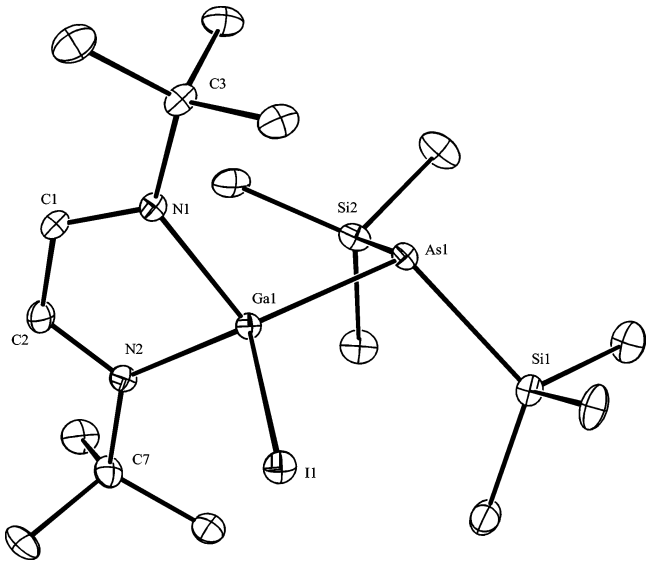

Figure 2. Thermal ellipsoid plot (30% probability surface) of the molecular structure of [(Bu^t-DAB)Ga{$As(SiMe_3)_2$}I] (**7**). Hydrogen atoms are omitted for clarity. Selected metrical parameters are listed in Table 2.

arsenido−gallane fragments, respectively. The Ga−P bond in **6** [2.2991(11) Å] is one of the shortest yet reported and can be compared with the mean Ga−P(terminal phosphide) distance for all previously reported structures (2.39 Å).[20] Moreover, it is very close to that in [(Bu^t)$_2$Ga{P(Mes*)-$SiPh_3$}] (Mes* = $C_6H_2Bu^t_3$-2,4,6) [2.295(3) Å] which has been postulated as having a weak Ga−P π-contribution to the bond.[21] Clearly, in **6** this cannot be the case as the gallium and phosphorus centers do not have trigonal planar geom-

(18) Becker, G.; Freudenblum, H.; Witthauer, C. *Z. Anorg. Allg. Chem.* **1982**, *492*, 37.

(19) (a) Atwood, D. A.; Atwood, V. O.; Cowley, A. H.; Jones, R. A.; Atwood, J. L.; Bott, S. G. *Inorg. Chem.* **1994**, *33*, 3251. (b) Brothers, P. J.; Wehmschulte, R. J.; Olmstead, M. M.; Ruhlandt-Senge, K.; Parkin, S. R.; Power, P. P. *Organometallics* **1994**, *13*, 2792. (c) Kühner, S.; Kuhnle, R.; Hausen, H.-D.; Weidlein, J. *Z. Anorg. Allg. Chem.* **1997**, *623*, 25.

(20) Determined from a survey of the Cambridge Crystallographic Database, September, 2004.

(21) Petrie, M. A.; Ruhlandt-Senge, K.; Power, P. P. *Inorg. Chem.* **1992**, *31*, 4038.

etries. Importantly, **7** possesses the shortest Ga−As single bond yet reported [2.3893(12) Å], which is significantly shorter than in related complexes, e.g. 2.421 Å average in $[Ga\{As(SiMe_3)_2\}_3]$.[22] The only shorter Ga−As interactions are the resonance stabilized double bonds [2.318(1) Å] in $[\{Li(THF)_3\}_2Ga_2\{As(SiPr^i_3)\}_4]$.[23]

Considering the formation of **5**−**7**, it is perhaps not surprising that the treatment of **3** with 4 equiv of $[LiE(SiMe_3)_2]$ (E = P, As) afforded compounds of the type $[(Bu^t\text{-DAB})Ga\{E(SiMe_3)_2\}_2]$, E = P (**8**) and As (**9**), in moderate yields (Scheme 1). Similarly, treating **6** or **7** with 1 equiv of $[LiE(SiMe_3)_2]$ led to these complexes. More unexpected was the result of the related reaction of **3** with 4 equiv of $[NaN(SiMe_3)_2]$. This led, reproducibly, to a moderate yield of the unusual coupled diradical product, **10**, as the only identifiable product.

The mechanism of formation of **10** has been investigated, and it is believed that the initial reaction product is $[(Bu^t\text{-DAB})Ga\{N(SiMe_3)_2\}_2]$ (cf. **8** and **9**). This is then thought to undergo an intramolecular transmethylation reaction to give the intermediate $[(Bu^t\text{-DAB})Ga\{N(SiMe_3)_2\}Me]$, **11**. This proposal has precedent in the reactions of $GaCl_3$ with either $[LiN(SiMe_3)_2]$[24] or $N(SiMe_3)_3$,[25] which both give rise to Si−C bond scissions and methyl migrations to the gallium centers. It must be said that, in the reaction mixture that gave **10**, we have not been able to isolate the expected elimination product, $\{(Me_3Si)NSi(Me)_2\}_2$. The final product, **10**, could be formed by deprotonation of the diazabutadiene backbone of one molecule of the intermediate, **11**, by the GaMe moiety of another (i.e. CH_4 elimination). This has been disproved by intentionally preparing **11** from the reaction of **5** with MeLi. The product was found to be stable toward the formation of **10**. Alternatively, **10** could be formed by deprotonation of the backbone of the intermediate, **11**, with excess $[NaN(SiMe_3)_2]$ in the reaction mixture. The resulting carbanion could then attack $[(Bu^t\text{-DAB})Ga\{N(SiMe_3)_2\}I]$, **5**, which must also be a reaction intermediate, to give **10** via NaI elimination. To test this hypothesis, an equimolar mixture of **5**, **11**, and $[NaN(SiMe_3)_2]$ in diethyl ether was warmed from −78 to 25 °C. Although the reaction was not clean, compound **10** was isolated from it in a low yield (ca. 10%). Presumably, similar coupling reactions were not observed in the preparations of **8** and **9** as the pyramidal geometries at their pnictogen centers (vide infra) circumvent close interactions between their gallium centers and $SiMe_3$ groups. This would be a likely prerequisite for methyl migration reactions to occur.

Crystals of **8**−**10** suitable for X-ray diffraction were grown from hexane solutions, and the molecular structures of **9** and **10** are shown in Figures 3 and 4, respectively. Compound **8** was found to be isostructural to **9,** and as a result, its molecular structure has been deposited as Supporting Information (see also Table 1). The asymmetric units of both **8** and **9** contain 1.5 crystallographically independent molecules which show no significant geometrical differences. Consequently, the structure of only the full independent molecule of each will be discussed here (Table 2). Both are monomeric

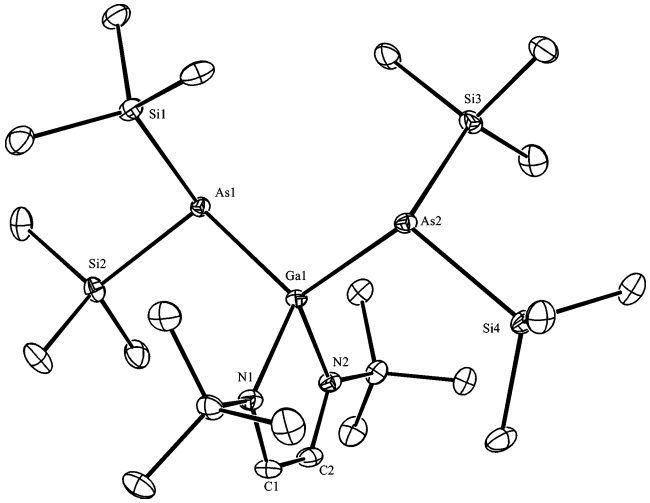

Figure 3. Thermal ellipsoid plot (30% probability surface) of the molecular structure of $[(Bu^t\text{-DAB})Ga\{As(SiMe_3)_2\}_2]$ (**9**). Hydrogen atoms are omitted for clarity. Selected metrical parameters are listed in Table 2.

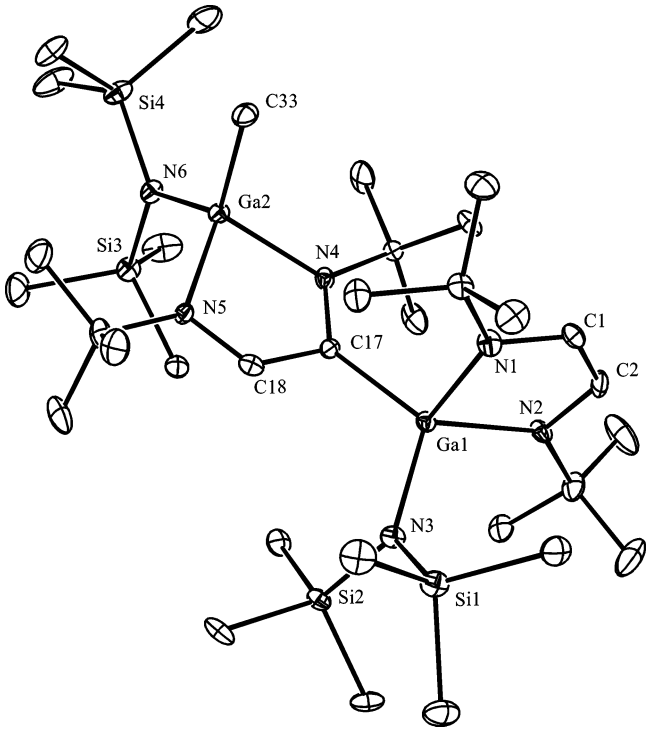

Figure 4. Thermal ellipsoid plot (30% probability surface) of the molecular structure of $[(Bu^t\text{-DAB})Ga\{N(SiMe_3)_2\}\{[CC(H)N_2(Bu^t)_2]Ga[N(SiMe_3)_2]\text{-}CH_3\}]$ (**10**). Hydrogen atoms are omitted for clarity. Selected bond lengths (Å) and angles (deg): Ga(1)−N(1) 2.036(5), Ga(1)−N(2) 1.986(5), Ga(1)−N(3) 1.910(5), Ga(1)−C(17) 2.023(6), Ga(2)−N(4) 1.990(5), Ga(2)−N(5) 1.972(5), Ga(2)−N(6) 1.909(4), Ga(2)−C(33) 1.981(6), N(1)−C(1) 1.333(8), N(2)−C(2) 1.344(8), N(4)−C(17) 1.359(8), N(5)−C(18) 1.315(8), C(1)−C(2) 1.382(9), C(17)−C(18) 1.432(8), N(1)−Ga(1)−N(2) 84.5(2), N(1)−Ga(1)−N(3) 116.5(2), N(1)−Ga(1)−C(17) 105.1(2), N(2)−Ga(1)−N(3) 107.2(2), N(2)−Ga(1)−C(17) 124.5(2), N(3)−Ga(1)−C(17) 115.5(2), N(4)−Ga(2)−N(5) 83.91(18), N(4)−Ga(2)−N(6) 118.4(2), N(4)−Ga(2)−C(33) 107.6(2), N(5)−Ga(2)−N(6) 115.5(2), N(5)−Ga(2)−C(33) 108.1(3), N(6)−Ga(2)−C(33) 118.1(2).

(22) Wells, R. L.; Self, M. F.; Baldwin, R. A.; White, P. S. *J. Coord. Chem.* **1994**, *33*, 279.
(23) von Hänisch, C.; Hampe, O. *Angew. Chem., Int. Ed.* **2002**, *41*, 2095.
(24) Luo, B.; Young, V. G., Jr.; Gladfelter, W. L. *J. Organomet. Chem.* **2002**, *649*, 268.
(25) Carmalt, C. J.; Mileham, J. D.; White, A. J. P.; Williams, D. J.; Steed, J. W. *Inorg. Chem.* **2001**, *40*, 6035.

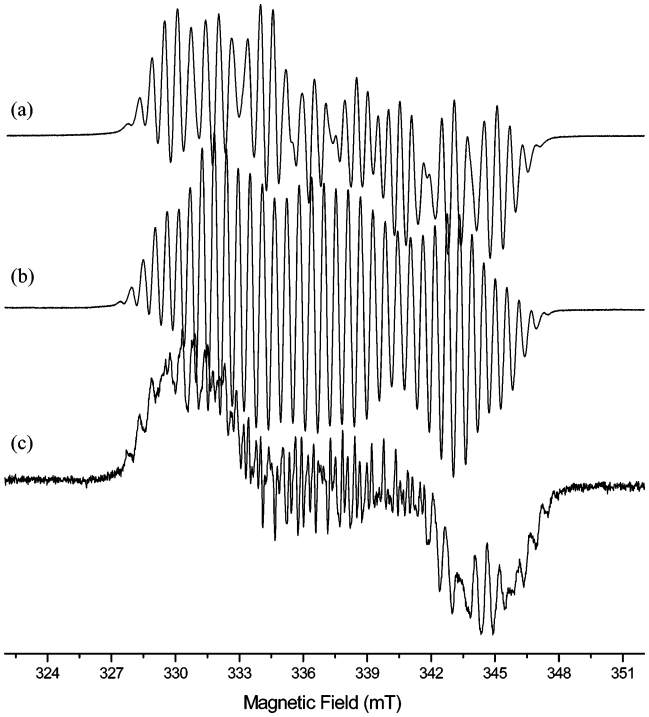

Figure 5. X-band EPR spectra of (a) **5**, (b) **6**, and (c) **7** recorded in hexane at 298 K.

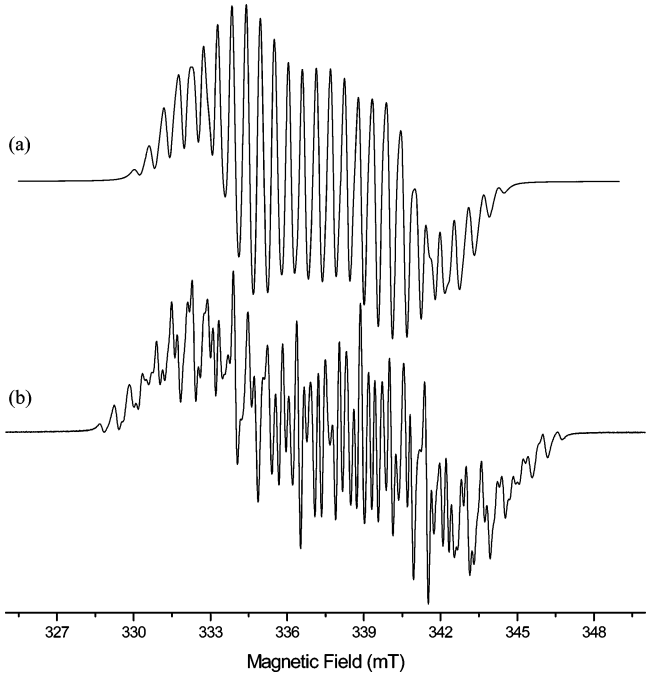

Figure 6. X-band EPR spectra of (a) **8** and (b) **9** recorded in hexane at 298 K.

with distorted tetrahedral geometries about their gallium centers. The geometries of the heterocyclic fragments are similar to those in **5**−**7**, while the average Ga−E bond lengths of **8** and **9** are significantly greater than those in **6** and **7**, presumably due to steric reasons.

The molecular structure of **10** confirms that a ligand coupling reaction has occurred in its formation. Both the heterocycles in this compound have similar geometries which imply significant delocalization over their diazabutadiene backbones (cf. **5**−**9**). Moreover, the two Ga−N(amide) bond lengths, 1.910(5) and 1.909(4) Å, are almost identical but greater than that in **5**. Finally, both Ga−C bonds [Ga(1)−C(17) = 2.023(6) Å, Ga(2)−C(33) = 1.981(6) Å] are in the normal range for such interactions.[20]

EPR Spectroscopic Studies. The EPR spectra of the paramagnetic complexes, **5**−**7**, were recorded at X-band frequency (9 GHz). The resulting room-temperature (298K) X-band spectra, recorded under identical conditions, for the complexes are shown in Figure 5a−c. A previous EPR study on the related complex [(Bu^t-DAB)GaI_2] revealed a relatively small degree of spin delocalization on the gallium nucleus, the observed hyperfine splittings being only 3.64 and 4.62 MHz for ^{69}Ga and ^{71}Ga, respectively (representing a 0.03% isotropic unpaired spin density on ^{69,71}Ga).[10] Hyperfine splittings to two equivalent nitrogen nuclei (24.14 MHz) and two α protons of the diazabutadiene ligand (3.92 MHz) and very weak couplings to the remote ^{127}I nuclei (3.64 MHz) were also identified in the EPR spectrum of that compound. As a result of these superimposed hyperfine patterns in the isotropic spectrum, the overall width of the final spectrum was 6.0 mT (168 MHz).

By comparison, the EPR spectra for **5**−**7** are much more complex and significantly wider, with spectral widths of 19.5, 20.1, and 20.5 mT, respectively. Attempts to successfully simulate the spectra using commercial simulation packages (e.g. SIMFONIA[13]) proved very difficult due to slight differences in ^{69,71}Ga hyperfine couplings and isotropic *g* values. For example, while an excellent fit with the outer lines could be achieved (i.e. essentially due to the wider contribution of the ^{71}Ga isotope), the shape of the inner lines was distorted due to overlap with the smaller ^{69}Ga component. This resulted from slight differences in the isotropic *g* values which we could not satisfactorily reproduce in the simulation. Nevertheless, the computer simulations did reveal an approximate hyperfine splitting of ca. 100 MHz to the ^{69,71}Ga nucleus of each compound, which represents ca. 0.7% spin density on the gallium nucleus. This can be rationalized in terms of a preferential polarization of the unpaired electron away from the $N_2C_2H_2$ fragment and toward the gallium nuclei due to the influence of the N-, P-, and As-centers. As a result, a small amount of the unpaired spin density can be found at the N-, P-, and As-nuclei, as manifested by a significantly increased number of lines in the EPR spectra. Despite the increased spin density on the gallium nuclei, the unpaired electron remains primarily localized on the diazabutadiene ligands of **5**−**7**, as confirmed by the relatively large ^{14}N and smaller ^{1}H EPR hyperfine splittings of ca. 25 MHz and ca. 3.59 MHz, respectively, which are similar to those for [(Bu^t-DAB)GaI_2]. The ^{1}H hyperfine couplings were more accurately determined by ENDOR spectroscopy, as discussed in the next section.

The room-temperature EPR spectra of **8** and **9** were also measured, and the resulting spectra are shown in Figure 6. The widths of the EPR spectra have decreased to 14.8 and 18.1 mT for **8** and **9**, respectively (cf. 20.1 and 20.5 mT for **6** and **7**). This result indicates that as slightly more electron spin is delocalized toward the two $P(SiMe_3)_2$ or $As(SiMe_3)_2$

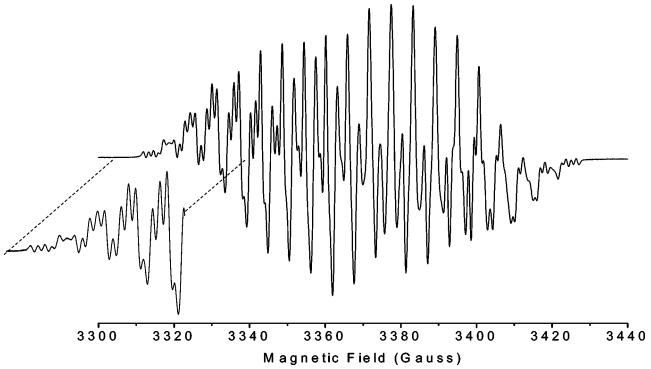

Figure 7. X-band EPR spectrum of **10** recorded in hexane at 298 K.

substituents, less spin remains on the gallium nucleus, and therefore smaller ^{69,71}Ga hyperfine splittings are observed, thus producing a decreased spectral width.

Figure 7 depicts the EPR spectrum for **10** recorded at 298 K. The spectrum is substantially different compared to the previous spectra, revealing a significantly altered structure for this paramagnetic complex. Despite the presence of two unpaired electrons in the two respective diazabutadiene ligands (i.e. a diradical), the resulting EPR spectrum is not typical of a system with an $S = 1$ triplet ground state and can best be interpreted as a composite spectrum with isotropic contributions from two $S = 1/2$ species. The frozen solution spectrum of **10** (see Supporting Information) revealed an easily identified quartet of ca. 3.0 mT (84 MHz) arising from the predominantly isotropic hyperfine splitting to one gallium nucleus, while the room temperature spectrum shows an unmistakable quartet feature (most clearly seen in the expanded outer wings of the spectrum) of 0.13 mT (3.64 MHz) separation which is due to a smaller hyperfine interaction with a second gallium nucleus. The former gallium splitting of ca. 84 MHz is approximately of the same order of magnitude as those observed for **5**−**7** while the latter coupling of 3.64 MHz is analogous to that observed for [(^{t}Bu-DAB)GaI$_2$]. The EPR spectrum and in particular the discrimination of hyperfine interactions to two independent gallium nuclei therefore confirm the identity of **10** as a dimeric gallium complex with two noninteracting $S = 1/2$ spin systems.

ENDOR Spectroscopic Studies. To extract further information on the unpaired spin densities in these complexes, the continuous wave (CW) ENDOR spectra were measured. The ENDOR spectra of the complexes in disordered solids (i.e. frozen solutions) are expected to be complicated by the broadened nature of the ENDOR response observed.[26] Due to absorptions from a range of orientations of the radical with respect to the direction of the magnetic field, the ENDOR lines arising from weak superhyperfine interactions to $I \neq 0$ nuclei will broaden and may become very weak. Unless the shape of the EPR spectrum is dominated by a particular dipolar interaction, there is little or no orientational selection in the ENDOR experiment and a powder-type

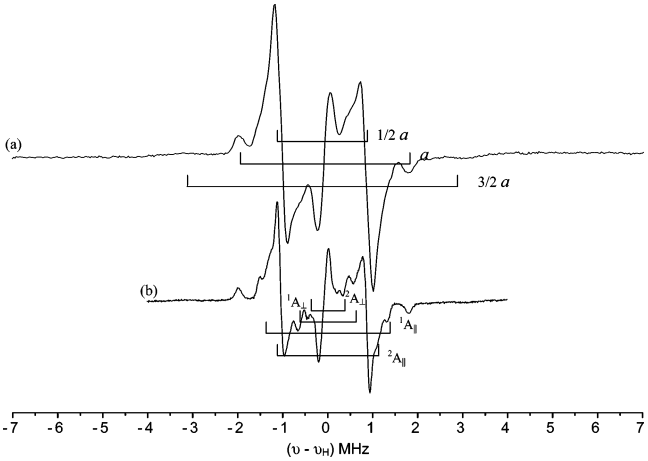

Figure 8. X-band ENDOR spectrum of **7** at (a) 250 kHz modulation depth and (b) 75 kHz modulation depth (recorded in CD_2Cl_2/C_7D_8 at 10 K).

spectrum is obtained.[27] This is the typical case expected for carbon-based organic free radicals, and narrow lines will only be obtained if the hyperfine anisotropy pertaining to the nucleus is small. For α protons, the anisotropy is about half of the hyperfine coupling, *a*, so that the principal values of the hyperfine tensor for α protons should occur near *a*/2, *a*, and 3/2*a*. The ENDOR spectra are thus expected to extend over a wider range (from *a*/2 to 3/2*a*) but with some build-up of intensity at the three principal values of the hyperfine tensor corresponding to those molecules with their respective principal axes oriented along the magnetic field.

The X-band ENDOR spectrum of **7** is shown in Figure 8. As the largest coupling (3/2*a*) is expected to produce a broad and weak signal, the ENDOR spectrum was recorded using a large rf modulation depth of 250 kHz (Figure 8a). The three principal values of the hyperfine tensor expected for an α-proton (*a*/2, *a*, and 3/2*a*) are clearly visible; the measured values are 1.897, 3.795, and 5.692 MHz, respectively (as shown by the stick diagram in Figure 8a). For α-protons the sign of the isotropic hyperfine coupling is expected to be negative, compared to β-protons where a positive sign is predicted.[26a,27c] The reason for the difference in sign relates to the different mechanisms of spin transfer from the π-center to such protons (spin polarization for α protons and hyperconjugation for β protons). Knowing the isotropic coupling is ca. 1.4 G (∼3.9 MHz) from the room-temperature EPR spectrum, and that this can be assigned a negative value, the three observed hyperfine tensor components of these protons, obtained from the frozen solution ENDOR spectrum, can therefore be assigned negative values (Table 3).

A number of additional peaks can also be detected in the CW ENDOR spectrum with pronounced smaller couplings. These couplings undoubtedly arise from weaker interactions to remote protons of the complex. To enhance the resolution of these additional lines, the spectrum was recorded using a

(26) (a) O'Malley, P. J.; Babcock, G. T. *J. Am. Chem. Soc.* **1986**, *108*, 3995. (b) Kevan, L.; Narayana, P. A. In *Multiple Electron Resonance Spectroscopy*; Dorio, M. M., Freed, J. H., Eds.; Plenum Press: New York, 1979; Chapter 6, p 229.

(27) (a) Hurreck, H.; Kirste, B.; Lubitz, W. *Electron Nuclear Double Resonance Spectroscopy of Radicals in Solution; Applications to Organic and Biological Chemistry*; VCH Publishers: Weinheim, Germany, 1988. (b) Gerson, F. *Acc. Chem. Res.* **1994**, *27*, 63. (c) Hyde, J. S.; Rist, G. H.; Ericksson, L. E. G. *J. Phys. Chem.* **1968**, *72*, 4269.

Table 3. Relative Sign and Magnitude (MHz) of the Hyperfine Couplings to the α-Protons and the Remote Protons of the *tert*-Butyl Groups of **7** As Determined by ENDOR Spectroscopy

protons	A_1	A_2	A_3	a_{iso}
α-H	−1.897	−3.795	−5.692	−3.795
tert-butyl	+2.859	−1.234	−1.234	+0.13
	+2.301	−0.863	−0.863	+0.19

lower rf modulation depth of 75 kHz (Figure 8b). The unresolved broad line at the nuclear Lamour frequency for ^{1}H (ν_N = 14.41 MHz at 3.385 mT) is due to a matrix ENDOR line. This line arises from almost purely dipolar couplings of the unpaired electron with surrounding (remote matrix) magnetic nuclei.[26b] The remaining lines can then be assigned to weak couplings with the remote protons of the *tert*-butyl groups (shown by the stick diagram in Figure 8b). In the case of *β*-protons, considerably less anisotropy is generally observed compared to α-protons. As a result, these interactions exhibit much stronger ENDOR lines in disordered solids. This is the situation for the remote *tert*-butyl protons in complex **10** which give rise to small hyperfine splittings (Figure 8b) which are slightly different for the two *tert*-butyl groups, thus implying a small inequivalency in the unpaired spin distribution on these substituents.

As discussed earlier in the EPR analysis, the presence of the electronegative elements in the $E(SiMe_3)_2$ substituents produced a noticeable redistribution of electron spin density onto the ^{69,71}Ga, ^{14}N, ^{31}P, and ^{75}As nuclei. However, it must be clearly noted that the theoretical isotropic hyperfine couplings of these elements are very large (435.68 and 553.58 mT for ^{69,71}Ga; 64.6 mT for ^{14}N; 474.8 mT for ^{31}P; 523.11 mT for ^{75}As), so even a very small spin density on the nuclei will produce an appreciable hyperfine coupling. We were unable to clearly detect any of these couplings in our CW ENDOR experiment. Despite the apparently large splittings to these nuclei observed in the EPR experiments, the unpaired electron distributions around the diazabutadiene ligand and the *tert*-butyl groups remain very similar for complexes **5**−**9**. This is confirmed by analysis of the ^{1}H ENDOR spectra for **5**−**7** shown in Figure 9 (analogous spectra were also recorded for **8** and **9**—see Supporting Information). The spectra (and therefore the associated hyperfine couplings responsible for the lines) for all complexes are virtually identical, revealing that the very weak couplings to the protons of the *tert*-butyl groups and the larger couplings to the α-protons remain predominantly unchanged over the series.

The CW ENDOR spectrum of **10** (see Supporting Information) is clearly different from those of **5**−**9** and can be interpreted in terms of two superimposed patterns arising, first, from the paramagnetic heterocycle containing the gallium center that bridges to the other heterocycle (producing a spectrum analogous to those observed for **5**−**9**) and, second, from the singly deprotonated heterocycle which displays a larger coupling to the remaining α-proton. The ENDOR spectrum supports the earlier claim that the EPR spectrum of **10** (Figure 7) reveals a substantially different structure for **10** compared to those of **5**−**9**.

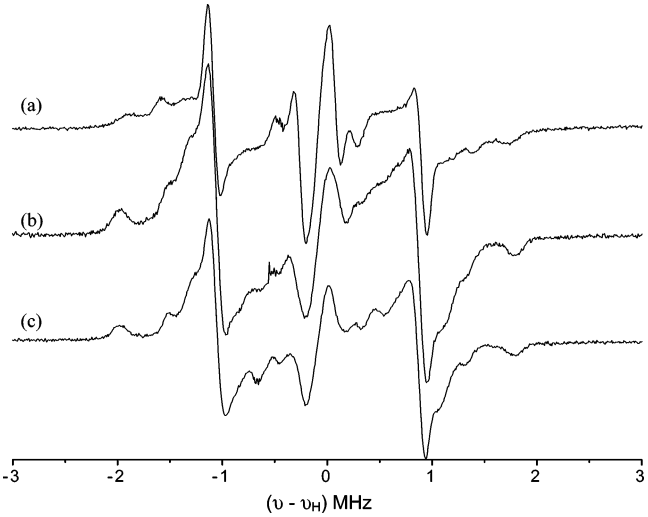

Figure 9. X-band ENDOR spectra of (a) **5**, (b) **6**, and (c) **7** recorded in CD_2Cl_2/C_7D_8 at 10 K.

Conclusions

In summary, the reactions of a gallium(II) dimeric complex, [{(Bu^t-DAB)GaI}$_2$], with the alkali-metal pnictides, [ME(SiMe$_3$)$_2$] (M = Li or Na; E = N, P, or As), have been carried out under a range of stoichiometries. The reactions have led to a series of paramagnetic gallium(III)−pnictide complexes, [(Bu^t-DAB)Ga{E(SiMe$_3$)$_2$}I] (E = N, P, As) and [(Bu^t-DAB)Ga{E(SiMe$_3$)$_2$}$_2$] (E = P, As). In addition, a novel gallium heterocycle coupling reaction has been observed and its mechanism explored. All prepared complexes have been characterized by X-ray crystallography, which in the case of one compound, **7**, has highlighted the shortest Ga−As single bond yet reported. Moreover, each of the paramagnetic compounds have been characterized in solution by EPR spectroscopy and the frozen-solution ^{1}H ENDOR spectra of several complexes have been acquired and analyzed. These spin resonance studies have enabled the estimation of the spin density over the molecular frameworks of the compounds. This has shown that although the EPR spectra of the various complexes appear very different, the spin densities on the peripheral atoms (e.g. the *tert*-butyl and E(SiMe$_3$)$_2$ substituents) do not significantly differ between the complexes, while most of the electron spin remains on their diazabutadiene backbones.

Acknowledgment. We thank the EPSRC (partial studentship for R.P.R. and postdoctoral fellowship for R.J.B.) for financial support and for funding the National ENDOR Service (Grant GR/R17980/01).

Supporting Information Available: Crystallographic data as CIF files for **5**−**10**, molecular structures of **6** and **8**, an EPR spectrum of **10** in hexane (100 K), and ENDOR spectra for **8**−**10** (10 K). This material is available free of charge via the Internet at http://pubs.acs.org.

IC0486825